Study of orbitally excited ($L = 1$) B mesons

Text for the blessed web page – CDF note 8945

The CDF Collaboration
URL http://www-cdf.fnal.gov
(Dated: August 7, 2007)

We study neutral orbitally excited B mesons in decays to $B^{(*)+}\pi^-$. The B^+ is reconstructed in two independent data samples in the decay modes $B^+ \to \mathrm{J}/\psi\mathrm{K}^+$, with $\mathrm{J}/\psi \to \mu^+\mu^-$, $B^+ \to \bar{D}^0\pi^+$, with $\bar{D}^0 \to K^+\pi^-$, and $B^+ \to \bar{D}^0\pi^+\pi^+\pi^-$, with $\bar{D}^0 \to K^+\pi^-$. From an unbinned maximum likelihood fit to the combined mass difference $Q = m(B\pi) - m(B) - m_\pi$, we extract the masses and width of the narrow B_1^0 and B_2^{*0} states:

$$m(B_1^0) = 5725.3^{+1.6}_{-2.1}\ (\mathrm{stat.})\ ^{+0.8}_{-1.1}\ (\mathrm{syst.})\ \mathrm{MeV/c^2}$$

$$m(B_2^{*0}) = 5739.9^{+1.7}_{-1.8}\ (\mathrm{stat.})\ ^{+0.5}_{-0.6}\ (\mathrm{syst.})\ \mathrm{MeV/c^2}$$

$$\Gamma(B_2^{*0}) = 22.1^{+3.6}_{-3.1}\ (\mathrm{stat.})\ ^{+3.5}_{-2.6}\ (\mathrm{syst.})\ \mathrm{MeV/c^2}$$

This is currently the most precise measurement of the narrow B^{**0} masses, and the first measurement of the B_2^{*0} width.

I. INTRODUCTION

This note describes a measurement of the first orbitally excited B mesons in $p\bar{p}$ collisions at $\sqrt{s} = 1.96$ TeV with the CDF II detector at the Fermilab Tevatron. The purpose of this analysis is to more precisely measure the properties of the excited B mesons, the spectroscopy of which has not been well-studied. There exist many theoretical predictions for the excited B states using different models of the heavy-light quark interactions, including heavy quark effective theories. Experimental confirmation of these predictions will lead to a better understanding of how heavy quarks and light quarks interact in bound states and help the development of non-perturbative QCD.

The B meson consists of a heavy b quark bound to a light u or d quark. In the limit of infinite b quark mass, the angular momentum and flavor of the light quark become good quantum numbers. The b quark has a spin angular momentum $J_Q = \frac{1}{2}$, while the light quark has a total angular momentum

$$J_l = \left| L \pm \frac{1}{2} \right| \tag{1}$$

where L is the orbital angular momentum of the light quark. The resulting physical hadron state has a total angular momentum of

$$\mathbf{J} = \left| J_l \pm \frac{1}{2} \right| \tag{2}$$

In the ground state of $L = 0$, $J_l = \frac{1}{2}$ and $\mathbf{J} = 0$ (B) or $\mathbf{J} = 1$ (B^*).

The first excited state of the B meson occurs when the light quark has an orbital angular momentum of $L = 1$. This leads to two isodoublets of excited states, one with $J_l = \frac{1}{2}$, $\mathbf{J} = 0$ or 1, and another with $J_l = \frac{3}{2}$, $\mathbf{J} = 1$ or 2. These four states are collectively referred to as B^{**}. The states belonging to the first doublet are called B_0^* and B_1^*, and they decay to $B^{(*)}\pi$ via a S-wave transition. Consequently, these states are expected to be very broad and have not yet been observed. The states belonging to the second doublet are called B_1 and B_2^*, and they decay to $B^{(*)}\pi$ via a D-wave transition; therefore these two states are much narrower than the $J_l = \frac{1}{2}$ states. The decay $B_1 \to B\pi$ is forbidden by angular momentum and parity conservation, while both $B_2^* \to B\pi$ and $B_2^* \to B^*\pi$ are allowed. Tab. I summarizes the $L = 1$ states and their decays. The B spectrum is depicted in Fig. 1. A similar spectrum exists for the B_s^{**0}, which consists of the b and s quarks. The narrow B_{s1}^0 and B_{s2}^{*0} have been measured in decays to $B^{(*)+}K^-$ [1]. When the kaon is misreconstructed as a pion, the B_s^{**} states will reflect into the B^{**} mass distribution.

TABLE I: Properties of the four orbitally excited ($L = 1$) B^{**} states.

State	J_l	$\mathbf{J}^P$	Width	Decay
B_0^*	$\frac{1}{2}$	0^+	broad	$(B\pi)$
B_1^*	$\frac{1}{2}$	1^+	broad	$(B^*\pi)$
B_1	$\frac{3}{2}$	1^+	narrow	$(B^*\pi)$
B_2^*	$\frac{3}{2}$	2^+	narrow	$(B\pi, B^*\pi)$

Decays to $B^*\pi$ are immediately followed by the decay of B^* to B by emission of a photon with energy $E(\gamma) = 45.78 \pm 0.35$ MeV/c^2 [2] virtually 100% of the time. These low energy photons cannot be separated from the large amount of other electromagnetic background sources in the CDF II detector; consequently, the reconstructed mass of the B^{**} states is decreased by the energy of this photon. This adds extra complication to the mass spectrum, as the $B_2^* \to B^*\pi$ mass peak will be displaced from the $B_2^* \to B\pi$ mass peak by the photon energy. The theoretical relative branching ratio of the two B_2^* decay modes is based on observations of the charm sector, and found to be [2]

$$\frac{BR(B_2^* \to B\pi)}{BR(B_2^* \to B^*\pi)} = 1.1 \pm 0.3 \tag{3}$$

The four orbitally excited B^{**} states exist for both $B^\pm$ and B^0, denoted respectively by $B^{**\pm}$ and B^{**0}. This note presents the reconstruction of B^{**0} states decaying to $B^{(*)\pm}\pi^\mp$. For ease of reference, B^{**} will be used in place of B^{**0} and B_1 and B_2^* in place of B_1^0 and B_2^{*0} from this point on. The narrow B_1^0 and B_2^{*0} states were first observed by the LEP experiments [3–5]. More recently, the narrow B^{**0} states have been precisely measured by the DELPHI [6] and DØ experiments [7]. A previous CDF II analysis also measured these states in 370 ± 20 pb^{-1} of data [8]. Thus far, no experiment has measured the widths of the B^{**0} mesons. One theorectical prediction for the narrow state widths is shown in Tab. II, and will be used in this analysis to constrain the B_1 width.

TABLE II: Theoretical predictions for the intrinsic widths of the two narrow B^{**} states [9].

Name	Prediction
$\Gamma(B_2^*)$	16 ± 6 MeV/c^2
$\Gamma(B_1)/\Gamma(B_2^*)$	0.9 (for pure D-wave)

II. DATA SAMPLE & EVENT SELECTION

The current analysis uses data collected with the CDF II detector by the $J/\psi \to \mu\mu$ and two displaced track triggers. The J/ψ trigger starts from two tracks which have information in the muon chambers and $p_{\rm T}$ larger than 1.5 (2.0) GeV/c^2 for different subdetectors and/or data taking periods. For the final online selection, the two tracks are required to have an opposite charge, an opening angle smaller than 135° and an invariant mass around the world average J/ψ mass. The two track trigger selects events based on the large impact parameter of the tracks coming from b hadron decays. It requires two tracks with an impact parameter in the range from 120 μm to 1 mm together with a minimal transverse momentum of each track and minimal scalar sum of the transverse momenta of the two tracks. This analysis utilizes data corresponding to an integrated luminosity of 1.7 fb^{-1} for the J/ψ trigger dataset and to 1.3 fb^{-1} for the two track trigger dataset.

The offline reconstruction starts with reconstructing B^+ candidates in the $J/\psi K^+$ and $\overline{D}^0(3)\pi$ decay modes with $J/\psi \to \mu^+\mu^-$ and $\overline{D}^0 \to K^+\pi^-$ [11]. The $B^+ \to J/\psi K^+$ is reconstructed from the J/ψ trigger data while the $B^+ \to \overline{D}^0(3)\pi$ is from the two track trigger data.

Reconstructed candidates are preselected using separate neural networks for each of the three channels. The neural networks are based on the NeuroBayes [10] package. They combine topological, kinematic, and particle identification quantities of the B^+ and its daughters. The neural networks for the $B^+ \to J/\psi K^+$ and $B^+ \to \overline{D}^0\pi^+$ are taken from the B_s^{**} analysis [1]. The network for $B^+ \to J/\psi K^+$ is trained on Monte Carlo events with the full CDF detector simulation for the signal patterns and data from the B^+ mass sidebands for the background patterns. For the $B^+ \to \overline{D}^0\pi^+$ channel we use the possibility to train the Neural Network with weights and use only data from both the B^+ mass signal and sideband regions, and subtract background statistically during neural network training. For selecting the $B^+ \to \overline{D}^0\pi^+\pi^+\pi^-$ we set up a further neural network which was trained using Monte Carlo events for the signal pattern and data from the upper B^+ mass sideband for the background pattern. The preselection is done by cutting on the neural network output, which is chosen to keep as much signal as possible, while removing a large part of the background. The invariant mass distributions of the B^+ candidates in the three channels are shown in Fig. 2. In total, 51500 B^+ signal events are selected in the $J/\psi K^+$ decay channel, 37300 in the $\overline{D}^0\pi^+$ channel, and 10200 in the $\overline{D}^0 3\pi$ channel.

The B^{**} candidates are constructed by combining B^+ candidates with a track which is assumed to be a pion. For the selection, three neural networks are trained on a combination of Monte Carlo events for the signal pattern and data for the background pattern. The data for the background pattern are taken from the entire Q range of 0 to 1.0 GeV/c^2, where the Q value is defined as $Q = m\,(B^+\pi^-) - m\,(B^+) - m_\pi^-$, with m denoting the invariant mass of the $B^+\pi^-$ pair, the B^+ candidate, and the pion respectively. Over the entire Q range, the B^{**} signal contribution in the background samples is marginal and can therefore be neglected. To avoid biasing the network training, the Monte Carlo events are generated with the same Q distribution as the data. The distributions of the neural network outputs can be found in Fig. 3. The plots show a good signal and background separation which is true for well-trained neural networks.

For the final selection we cut on the number of candidates per event and on the output of the neural networks. The cut on the number of candidates is fixed to be the same for all three B^+ decay channels, and requires fewer than six B^{**} candidates in an event. The cut on the neural network output is chosen to maximize $N_{MC}/\sqrt{N_{data}}$, which is proportional to the significance $S/\sqrt{S+B}$. The optimization is done by counting the number of Monte Carlo events N_{MC} and the number of data events N_{data} in the Q value range from 0.2 GeV/c^2 to 0.4 GeV/c^2 for a given cut on the network output. The best cut is found to be 0.5 for the decay $B^{**0} \to B^+\pi^- \to (J/\psi K^+)\pi^-$, 0.7 for $B^{**0} \to B^+\pi^- \to (\bar{D}^0\pi^+)\pi^-$, and 0.75 for $B^{**0} \to B^+\pi^- \to (\bar{D}^0\pi^+\pi^+\pi^-)\pi^-$. Fig. 4 shows the Q distributions of the B^{**} candidates for these network cuts.

In view of the combined fit performed for the analysis, we also optimized the selection using the combined significance, which is a function of all three network outputs. In this case, the cuts on the network outputs are optimized simultaneously when the combined significance is maximized. The best cuts on the network outputs for the combined significance are 0.85 for the decay $B^{**0} \to B^+\pi^- \to (J/\psi K^+)\pi^-$, 0.7 for $B^{**0} \to B^+\pi^- \to (\bar{D}^0\pi^+)\pi^-$, and 0.75 for

$B^{**0} \to B^+\pi^- \to (\bar{D}^0\pi^+\pi^+\pi^-)\pi^-$. Fig. 5 shows the Q distributions of the B^{**} candidates at these network cuts.

III. B^{**} FIT DESCRIPTION

To reduce the effects of detector and mass resolution, we fit the B^{**} mass difference Q. The expected B^{**} signal structure was described in Sec. I. We fit for three peaks, one for each of the decays $B_2^* \to B\pi$, $B_2^* \to B^*\pi$, and $B_1 \to B^*\pi$. Each peak is modeled as a non-relativistic Breit-Wigner convoluted with a double Gaussian detector resolution model. Theoretical predictions enter into the fit as Gaussian constraints to the likelihood. These predictions and their Gaussian uncertainties are:

- Ratio of B_1 and B_2^* widths: $\frac{\Gamma(B_1)}{\Gamma(B_2^*)} = 0.9 \pm 0.2$
- Energy of B^* photon: $E(\gamma) = 45.78 \pm 0.35$ MeV/c^2
- Ratio of B_2^* branching fractions: $\frac{BR(B_2^* \to B\pi)}{BR(B_2^* \to B^*\pi)} = 1.1 \pm 0.3$
- Number of misreconstructed B_{s1}^0 events in combined data: 24 ± 12
- Number of misreconstructed B_{s2}^{*0} events in combined data: 62 ± 31

We derive the shape of misreconstructed B_s^{**} events from Monte Carlo simulations, and fix these shapes in the fit to data. The number of misreconstructed B_s^{**} events is constrained to expectations from the B_s^{**} analysis [1]. The background is modeled by a smooth function, a power law times an exponential. There is a small fixed component to the background at high mass, but the background shape under the signal region is left floating in the fit to data. Tests of the fit show that it is stable, with negligible fit bias on the B^{**} signal parameters.

To cross-check that the B^{**} signal is consistent in each B^+ decay channel, we first fit each of the individually optimized B^+ samples separately. The fit results to data are shown in Fig. 6. The B^{**} signal parameter values are given in Tab. III. The signal location is consistent among the three channels within statistical uncertainties.

TABLE III: B^{**} signal parameters from fits to each of the B^+ decay channels separately. Overall the signal location is consistent among the decay channels. These fits are only used as a cross-check of the final B^{**} fit to the combined events.

Parameter	$J/\psi K$ channel	$\bar{D}^0\pi$ channel	$\bar{D}^0 3\pi$ channel
B_2^* Q (MeV/c^2)	321 ± 3	320 ± 3	324 ± 3
$m(B_2^*) - m(B_1)$ (MeV/c^2)	13 ± 4	14 ± 3	17 ± 3
$\Gamma(B_2^*)$ (MeV/c^2)	35 ± 9	20 ± 6	21 ± 6
Number of $B_1 \to B^*\pi$ events	260 ± 102	208 ± 57	145 ± 49
Number of $B_2^* \to B\pi$ events	454 ± 78	127 ± 31	112 ± 24

IV. RESULTS

For the final B^{**} fit, we combine the events in all B^+ decay channels after optimizing the signal samples for the combined significance. The result of this fit is shown in Fig. 7. The χ^2 probablity of the fit is 78% in the range $Q \in [0., 0.5]$ GeV/c^2, and 53% over the full range $Q \in [0., 1.0]$ GeV/c^2. The fit results for the B^{**} signal parameters are shown in Tab. IV. The data is consistent with having only two signal peaks of widely different widths, so the interpretation of three signal peaks is motivated by theoretical predictions. The signal is consistent with theoretical predictions, including those entered as Gaussian constraints in the likelihood.

V. SYSTEMATIC UNCERTAINTIES

There are three components to the systematic uncertainties on the measurement: mass scale systematics, systematic uncertainties due to assumptions used in the fit, and systematic uncertainties due to the choice of background model.

To determine the mass scale uncertainty, we compare CDF II mass measurements of the D^*, Σ_c^0, Σ_c^{++}, Λ_c^*, and $\psi(2s)$ particles with the world average values quoted in the PDG [2]. We plot the difference between the CDF and

TABLE IV: Final B^{**} signal parameters from the fit to the combined events. We use asymmetric uncertainties as the likelihood is asymmetric for some parameters.

Parameter	Value	Stat. uncertainties
B_2^* Q (MeV/c^2)	321.2	$(+1.7, -1.8)$
$\Gamma(B_2^*)$ (MeV/c^2)	22.1	$(+3.6, -3.1)$
$m(B_2^*) - m(B_1)$ Q (MeV/c^2)	14.6	$(+2.2, -2.5)$
Number of $B_1 \to B^*\pi$ events	496	$(+72, -66)$
Number of $B_2^* \to B\pi$ events	357	$(+46, -44)$

PDG mass measurements as a function of the Q value of the decay, and fit the graph to a linear function. This function is evaluated at the B^{**} Q values to estimate the systematic uncertainty. This is a small systematic uncertainty.

Assumptions made in the fit are included as Gaussian constraints added to the likelihood, as described in Sec. III. Thus, the systematic uncertainty due to these assumptions is already included in the statistical uncertainty on each parameter in the fit. To separate the statistical and systematic uncertainties in the fit, we refit the data with the constrained parameters fixed. For this fit, the only component of the uncertainties is the statistical uncertainty. To find the systematic uncertainty, we subtract in quadrature the statistical uncertainties for the two fits to data, one with the constrained parameters floating and one with them fixed. This is the largest systematic uncertainty on all parameters.

To estimate the uncertainty due to the choice of background model, we generate a set of 1000 pseudo-experiments using an alternate background parameterization. Each sample is fit with both the default fit and the fit with an alternate background model. We then take the difference between the parameter values in the varied fit and the default fit as the systematic uncertainty due to the background model. We model this difference with a Gaussian and take the mean of the Gaussian as the systematic uncertainty. This is a small systematic uncertainty.

VI. SUMMARY

Using three fully reconstructed decay modes, $B^{**0} \to B^+\pi^- \to (J/\psi K^+)\pi^-$, $B^{**0} \to B^+\pi^- \to (\bar{D}^0\pi^+)\pi^-$, and $B^{**0} \to B^+\pi^- \to (\bar{D}^0\pi^+\pi^+\pi^-)\pi^-$, we observe the two narrow B^{**0} states in agreement with previous measurements and theoretical predictions. The results of this study show:

- $m(B_2^{*0}) - m(B) - m_\pi = 321.2^{+1.7}_{-1.8}$ (stat.) $^{+0.3}_{-0.4}$ (syst.) MeV/c^2
- $m(B_2^{*0}) - m(B_1^0) = 14.6^{+2.2}_{-2.5}$ (stat.) $^{+0.7}_{-0.9}$ (syst.) MeV/c^2
- $\Gamma(B_2^*) = 22.1^{+3.6}_{-3.1}$ (stat.) $^{+3.5}_{-2.6}$ (syst.) MeV/c^2

The ratio of the widths, $\frac{\Gamma(B_1)}{\Gamma(B_2^*)}$, while not measured in this analysis, is consistent with a theoretical prediction of 0.9.

The B_2^* Q value is converted into an absolute mass by adding the B^+ and charged pion masses to the Q value. There is a small uncertainty on the B^+ world average mass, $B^+ = 5279.1 \pm 0.4$ MeV/c^2 [2], which is added in quadrature to the systematic uncertainty of the absolute B_2^* mass. The B_1 absolute mass may be obtained by subtracting $m(B_2^{*0}) - m(B_1^0)$ from the B_2^* Q value, and then adding the B^+ and charged pion masses. This results in absolute mass values of:

- $m(B_1^0) = 5725.3^{+1.6}_{-2.1}$ (stat.) $^{+0.8}_{-1.1}$ (syst.) MeV/c^2
- $m(B_2^{*0}) = 5739.9^{+1.7}_{-1.8}$ (stat.) $^{+0.5}_{-0.6}$ (syst.) MeV/c^2

The number of events in each peak is measured to be:

- $N(B_1^0 \to B^{*+}\pi^-) = 496^{+72}_{-66}$ (stat.) $^{+113}_{-97}$ (syst.)
- $N(B_2^{*0} \to B^+\pi^-) = 357^{+46}_{-44}$ (stat.) $^{+34}_{-33}$ (syst.)
- $N(B_2^{*0} \to B^{*+}\pi^-) = 328^{+46}_{-44}$ (stat.) $^{+34}_{-33}$ (syst.)

The ratio $\frac{BR(B_2^* \to B\pi)}{BR(B_2^* \to B^*\pi)}$, while not measured in this analysis, is consistent with the theoretical prediction of 1.1.

This is the most precise measurement of the narrow B^{**0} states to date. This is also the first measurement of the B_2^{*0} width.

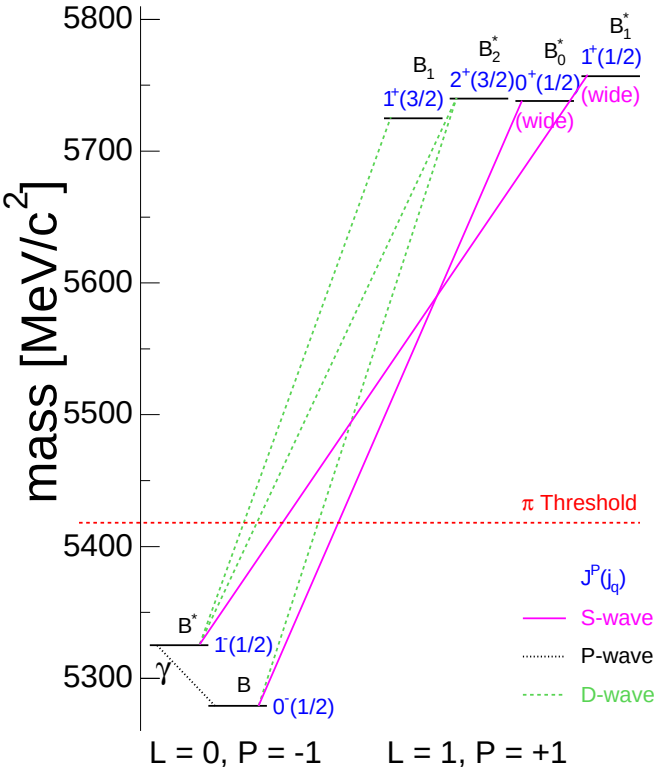

FIG. 1: Predicted spectrum and dominant decays of the lowest lying B meson states.

Acknowledgments

We thank the Fermilab staff and the technical staffs of the participating institutions for their vital contributions. This work was supported by the U.S. Department of Energy and National Science Foundation; the Italian Istituto Nazionale di Fisica Nucleare; the Ministry of Education, Culture, Sports, Science and Technology of Japan; the Natural Sciences and Engineering Research Council of Canada; the National Science Council of the Republic of China; the Swiss National Science Foundation; the A.P. Sloan Foundation; the Bundesministerium für Bildung und Forschung, Germany; the Korean Science and Engineering Foundation and the Korean Research Foundation; the Particle Physics and Astronomy Research Council and the Royal Society, UK; the Institut National de Physique Nucleaire et Physique des Particules/CNRS; the Russian Foundation for Basic Research; the Comisión Interministerial de Ciencia y Tecnología, Spain; the European Community's Human Potential Programme under contract HPRN-CT-2002-00292; and the Academy of Finland.

[1] CDF Collaboration, "Observation of orbitally excited $L = 1$ B_s mesons", CDF Note 8468 (2006).
[2] W. M. Yao *et al.* [Particle Data Group], "Review of particle physics," J. Phys. G **33**, 1 (2006).
[3] ALEPH Collaboration, "Resonant Structure and Flavor-tagging in the $B\pi^{\pm}$ System Using Fully Reconstructed B Decays," contribution to the International Europhysics Conference on High Energy Physics, Brussels, Belgium (1995).
[4] DELPHI Collaboration, "Observation of Orbitally Excited B Mesons," CERN-PPE/94-210 (1994); DELPHI Collaboration, "Observation of Orbitally Excited B and B_s Mesons," DELPHI 95-105 PHYS 540 (1995).
[5] R. Akers *et al.* [OPAL Collaboration], "Observations of pi - B charge - flavor correlations and resonant B pi and B K production," Z. Phys. C **66**, 19 (1995).
[6] Delphi Collab., Z. Albrecht et al., DELPHI 2004-025 CONF 700; Z. Albrecht, *Analysis of Excited B-Mesons*, PhD-Thesis, IEKP-KA/03-16, Universität Karlsruhe, 2003; M. Moch, *Study of B^+-Mesons and of Excited b-Hadron Properties*, PhD-Thesis, IEKP-KA/2004-16, Universität Karlsruhe, 2004. Both theses available at `http://www-ekp.physik.uni-karlsruhe.de/pub/web/thesis`.
[7] V. M. Abazov *et al.*, "Observation and Properties of L=1 B_1 and B_{2*} Mesons," arXiv:0705.3229 [hep-ex].

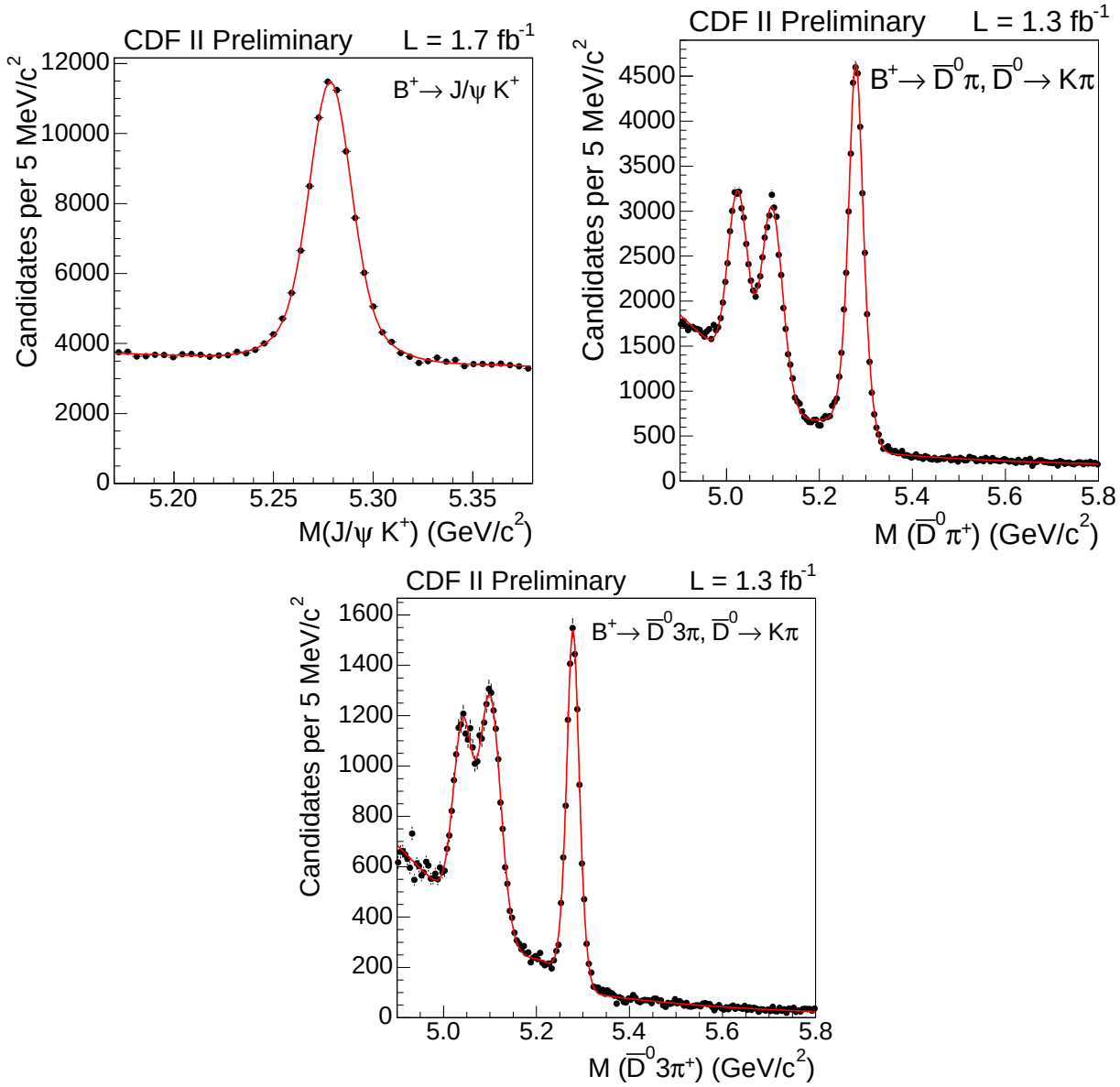

FIG. 2: The invariant mass distributions of the B^+ candidates at the best neural network cuts.

[8] CDF Collaboration, "Observation of orbitally excited ($L = 1$) B mesons", CDF note 7938 (2005).
[9] A. F. Falk and T. Mehen, "Excited heavy mesons beyond leading order in the heavy quark expansion," Phys. Rev. D **53**, 231 (1996) [arXiv:hep-ph/9507311].
[10] M. Feindt, A Neural Bayesian Estimator for Conditional Probability Densities, physics/0402093, 2004; M. Feindt and U. Kerzel, Nucl. Instrum. Methods A **559**, 190 (2006).
[11] Unless otherwise noted, any reference to a specific charge state implies the charge conjugate state as well.

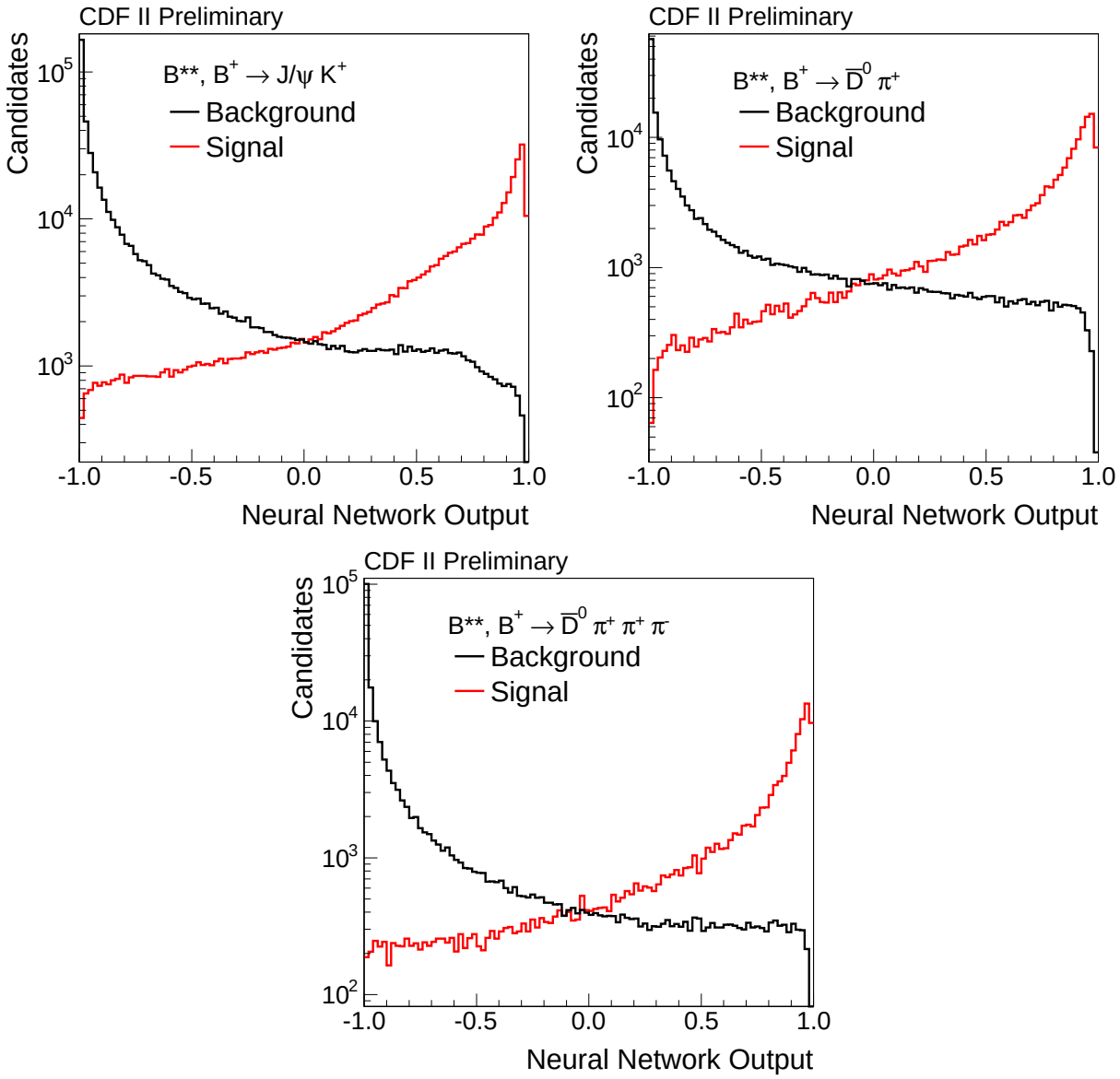

FIG. 3: The distributions of the neural network outputs for signal (red) and background (black) events using the training samples.

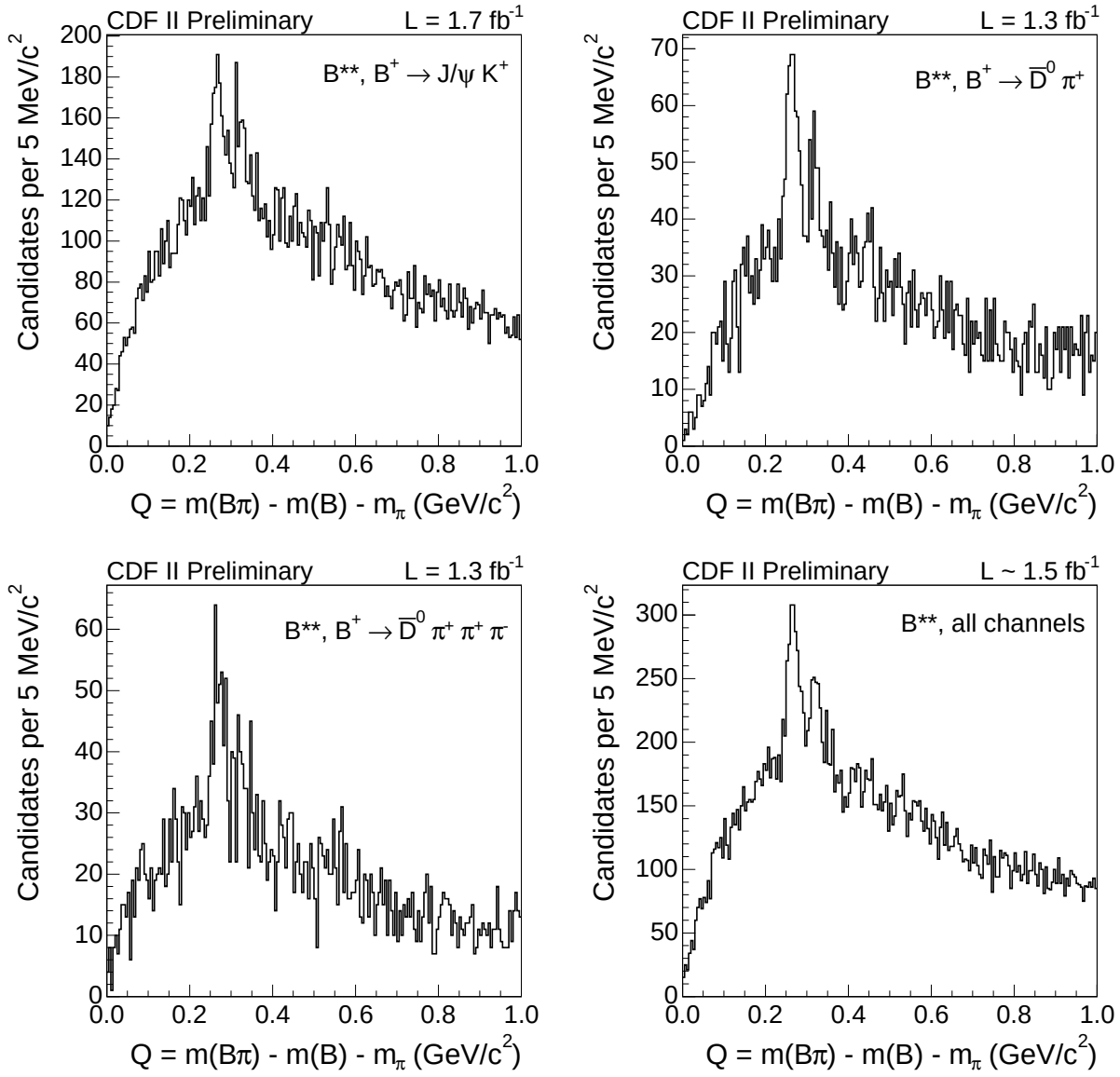

FIG. 4: The Q distributions of the B^{**} candidates at the best neural network cuts when channels are optimized separately. The final plot shows the events of all three channels combined.

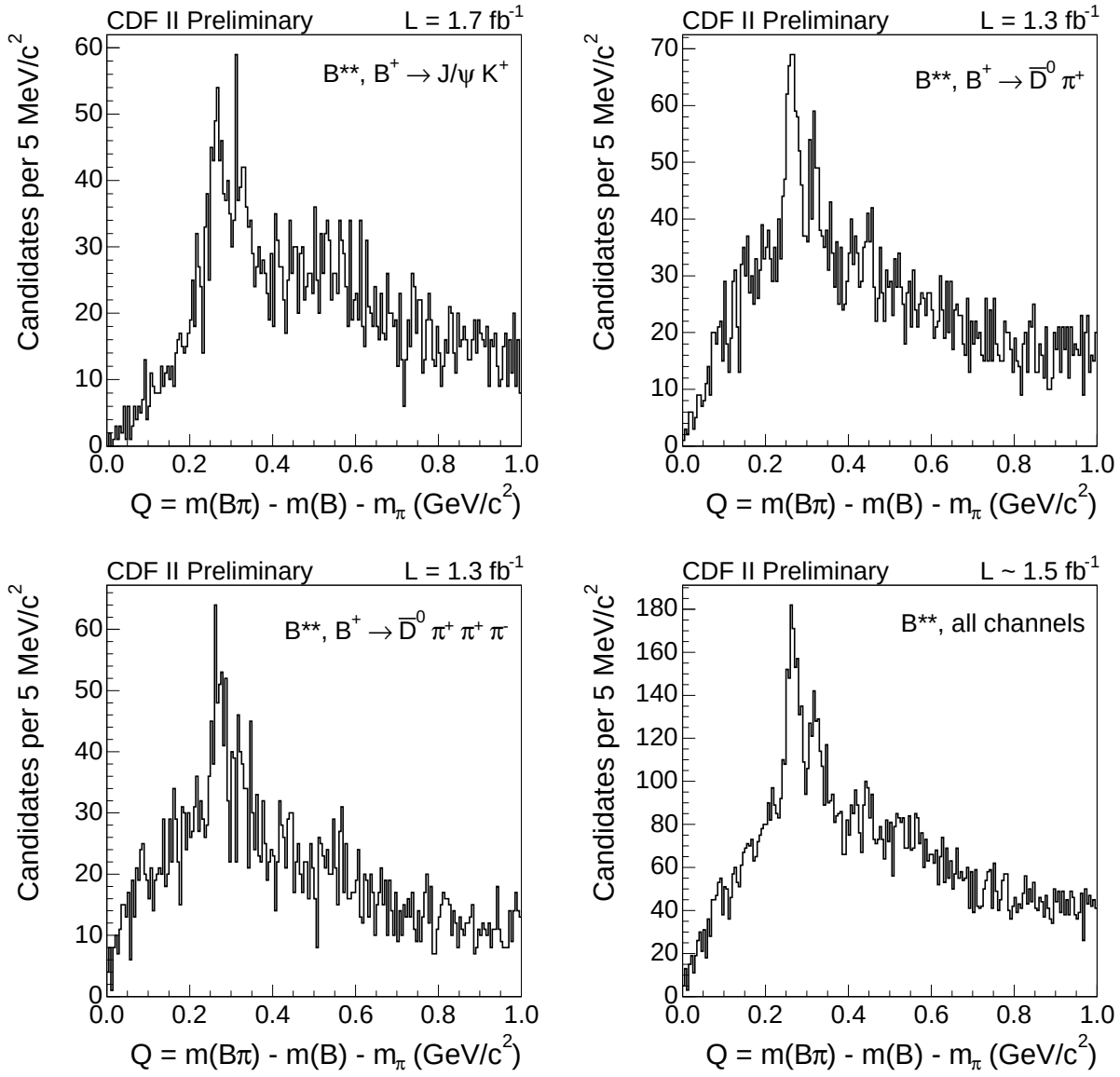

FIG. 5: The Q distributions of the B^{**} candidates at the best neural network cuts when channels are optimized simultaneously. The final plot shows the events of all three channels combined.

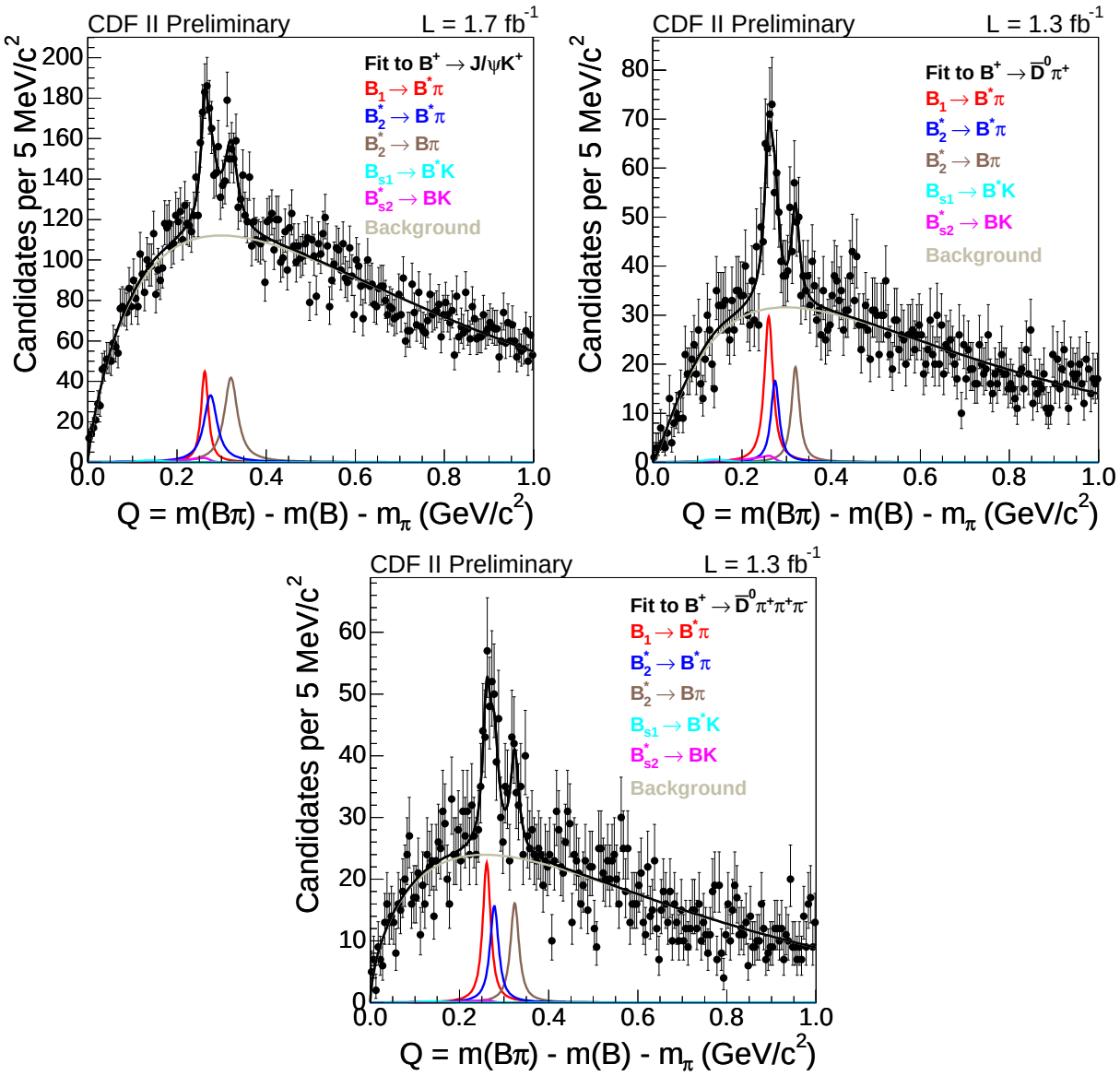

FIG. 6: Individual B^{**} fits to the three B^+ samples. From left to right: $B^{**0} \to B^+\pi^- \to (J/\psi K^+)\pi^-$, $B^{**0} \to B^+\pi^- \to (\bar{D}^0\pi^+)\pi^-$, and $B^{**0} \to B^+\pi^- \to (\bar{D}^0\pi^+\pi^+\pi^-)\pi^-$. These fits are used as cross-checks of the final combined fit, to check that the B^{**} signal is consistent in all three channels separately.

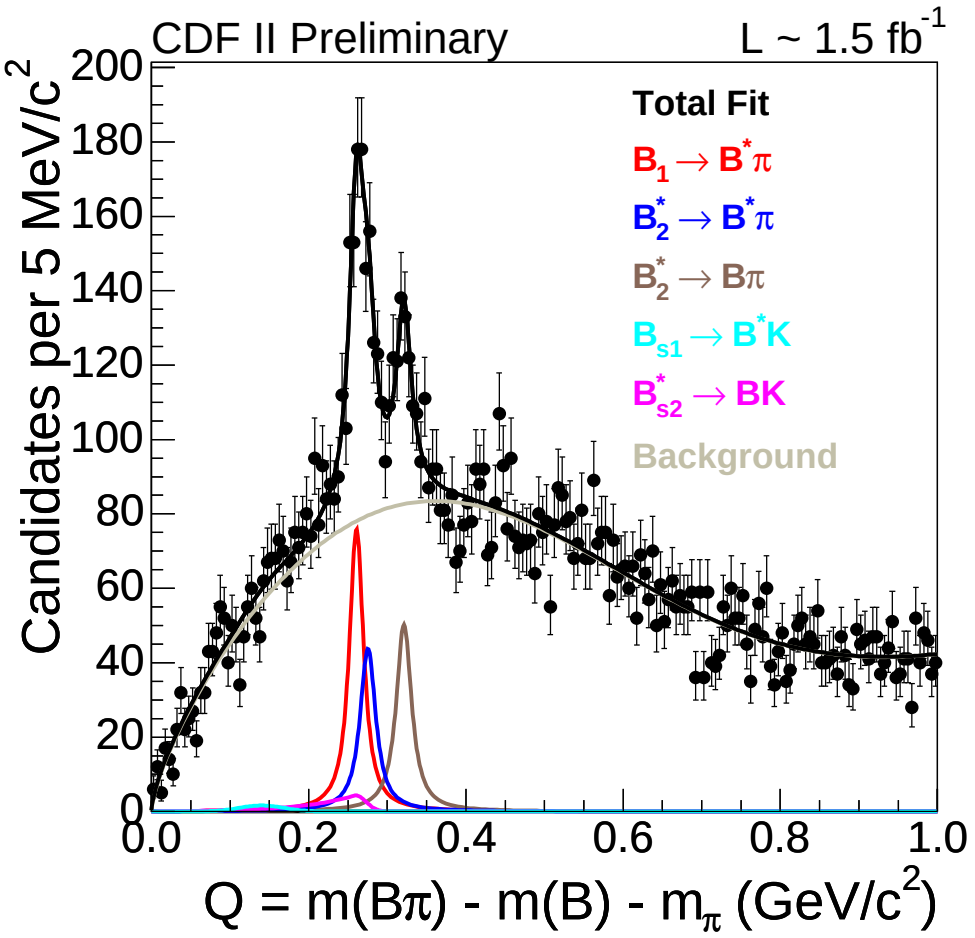

FIG. 7: B^{**} fit to the combined data sample. The three B^{**} signal peaks are shown separately.